Int. J. Simul. Multidisci. Des. Optim. **4**, 149-158 (2010)
© ASMDO 2010
DOI: 10.1051/ijsmdo/2010019

Available online at:
http://www.ijsmdo.org

Optimal Modeling Study of Flooding Phenomenon in Urban Area (Dam break case)

M. Rezoug[1,A], R.El Meouche[1], R. Hamzaoui[1], J.F Khreim[1], Z.Q Feng[2], D. Bassir[1]

[1] FIT / ESTP/ Constructibility Research Institute. 28, avenue du Président Wilson - 94234 Cachan cedex, France.
[2] EVRY Laboratory *LME-Evry*. Evry University, 40 rue du Pelvoux, 91020 Evry, France.

Received 30 May 2010, Accepted 25 September 2010

Abstract – In this paper a numerical study of urban flooding caused by dam break has been undertaken. **Problem statement:** This study illustrated the influence of the different versions of K-epsilon turbulence model on the water flow behavior, predicted by Computational Fluid Dynamic (CFD) and validated through experiment. **Approach:** The water velocity, free surface profile and also secondary circulation flow along with the pressure through the city are simulated and proved. **Results:** Results are obtained with numerical simulation using standard k-epsilon, are relatively good agreement with the experimental results. **Conclusion/Recommendations:** In the present study, the velocity and the water depth are investigated to check the real capabilities of a 3D numerical code ANSYS-CFX and especially to define the optimal parameters (Mesh, boundary conditions, turbulence model,) able to simulate the flow behavior through the complex urban area, with the best accuracy.

Keywords: Urban flooding; Turbulence models; Free surface flow; VOF; Computational Fluid Dynamic (CFD); ANSYS-CFX.

1 Introduction

Various computational fluid dynamics methods have already been used in order to simulate flood progress in cities [1-4]. In recent years there have been advances in modelling the interaction between sewer models and models describing the flow on the surface. Two dimensional models originally developed for use in estuaries and oceanic modeling has been modified to interact with the drainage system, i.e. MIKE 2 [5], TUFLOW [6] and RMA-2 [7]. Other models have been developed specifically to describe overland flooding, such as DELFT-FLS [8] and GIS based pathway models [9]. This will allow for more complex systems to be better described and modeled. The results are encouraging but there is still a lack of knowledge in the accuracy of the risk assessment.

In view of the flow, singularities, sewage systems, the presence of storage volumes (water entry through doors of buildings, cellars, gardens, lawns, parking garages, etc.) are the origin of losses of hydraulic head due to the turbulence created. These losses are difficult to quantify, as they are tributary of the flow properties and the fluid, they also depend on the precise shape of an obstacle, its orientation and its surface roughness, etc. Note the flow near an obstacle has a fully three-dimensional structure with a strong component of vertical velocity, this implies that near the obstacles, the use of a 2D codes based on SaintVenant equations is not strictly correct [10, 11].

The aim of this work is to check the real capabilities of a 3D numerical code ANSYS-CFX to simulate an urban flood. To find good results, three mesh types (hexahedral, tetrahedral with refinement and tetrahedral with inflation) have taken and applied to three turbulence models for each mesh type (Standard k-ε, RNG and Realizable k-ε model). To validate numerical results, an experimental test case of flood in a simplified city, have been taken as a base of comparison [12], it consists to study the flow around a buildings where the reflections of the wave on the walls and recirculation behind the obstacles are two parameters which have a major importance. The comparisons between the experimental and numerical records should permit to check the difficulties remaining when simulating an urban flood numerically.

2 Presentation of the test case

The experimental device is located at the Catholic University of Louvain (Belgium) [12]. This is a great channel with a length of 36 meters and a width of 3.6 meters with a horizontal bottom (Figure 1). A narrowing of a section and a door are arranged in the channel to simulate a dam break.

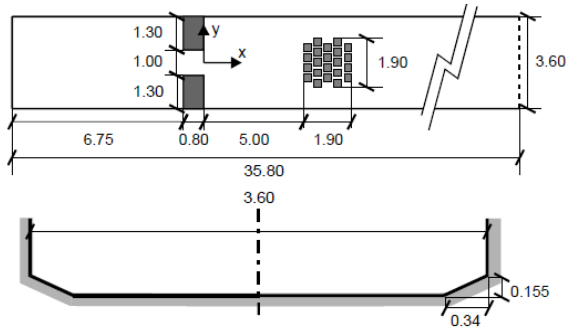

Fig. 1. Experimental device, dimensions of the channel (meters) and simplified arrangement of the city (J. Lhomme et al., 2006)

In this study, a Permanent flow (95 L / s) is simulated by keeping the door opened and pumping water from one end to the other of the channel. A simplified city is arranged in the channel with a staggered arrangement of buildings. The coefficient of Strickler channel is equal to100 m1/3/s.

[a] Corresponding author: rezoug@profs.estp.fr

Two methods of measurement have been used. The RTDs (Resistance Temperature Detectors) allow the recording of changes in depth, and digital imaging technique was used to track the movement of tracers (polystyrene beads) on the surface of the water, and allow obtaining the field of velocity at the surface [13].

3 Three-dimensional multiphase model

The three-dimensional multiphase approach is based on the numerical resolution of the incompressible Navier-Stokes equations. To maintain the multiphase nature of the flow, there are currently two approaches widely used: the Euler-Lagrange approach and the Euler-Euler approach. In the latter approach, the different phases are taken into account by considering that the volume of a phase cannot be occupied by other phases. Then the concept of phase volume fractions as continuous functions of space and time is introduced.
In this paper, the so-called Volume of Fluid (VOF) method is used [14, 15]. The VOF method is a surface tracking technique applied to a fixed Eulerian mesh, in which a specie transport equation is used to determine the relative volume fraction of the two phases, or phase fraction, in each computational cell. Practically, a single set of Reynolds- averaged Navier-Stokes equations is solved and shared by the fluids and for the additional phase, its volume fraction γ is tracked throughout the domain.
Therefore, the full sets of governing equations for the fluid flow are [16]:

$$\frac{\partial}{\partial x_i}(\rho_m u_i) = 0 \tag{1}$$

$$\frac{\partial \rho_m u_i}{\partial t} + \frac{\partial}{\partial x_i}(\rho_m u_i u_j) = -\frac{\partial p}{\partial x_j} + \frac{\partial}{\partial x_i}\left(\mu_m \left[\frac{\partial u_i}{\partial x_j} + \frac{\partial u_j}{\partial x_i}\right]\right)$$

$$+\frac{\partial}{\partial x_i}(-\rho_m \overline{u_i' u_j'}) + \rho_m g_j \tag{2}$$

$$\frac{\partial \alpha}{\partial t} + \vec{u}.\nabla\alpha = 0 \tag{3}$$

For the incompressible phase volume fraction, α the following three conditions are possible:

- $0 < \alpha < 1$: when the infinitesimal volume contains the interface between the q-th fluid and one or more other fluids;
- $\alpha = 0$: volume occupied by air;
- $\alpha = 1$ volume occupied by water.

The nature of the VOF method means that an interface between the species is not explicitly computed, but rather emerges as a property of the phase fraction field. Since the phase fraction can have any value between 0 and 1, the interface is never sharply defined, but occupies a volume around the region where a sharp interface should exist.

3.1 Turbulence modeling

Modeling turbulent flow in a multi-phase model is highly challenging because of the complexity associated with strong turbulence anisotropy, streamline curvature, and rotation.

In present calculations fully homogeneous buoyant models are used with air and water as continuous fluids because of a requirement for more accurate representation of the turbulent transport of momentum in order to achieve an improved prediction of the flow field around obstacles. This goal may be realized through the use of three mathematical models of turbulence namely the model (Standard k-ε, RNG k-ε and Realizable k-ε model).

- The main differences between the three models are:
- The turbulent Prandtl number governing the turbulent diffusion.
- The production and destruction terms in the equation for epsilon.

The methods to calculate the turbulent viscosity.

3.1.1 Standard k-ε model

This standard model has been proposed b is based on the concept Bousinesq (1977). The two equations of this model are [17, 18]:

For turbulent kinetic energy *K*

$$\frac{\partial}{\partial t}(\rho k) + \frac{\partial}{\partial x_i}(\rho k u_i) = \frac{\partial}{\partial x_j}\left[\left(\mu + \frac{\mu_t}{\sigma_k}\right)\frac{\partial k}{\partial x_j}\right]$$

$$+G_k + G_b - \rho\varepsilon - Y_M + S_K \tag{4}$$

For dissipation ε

$$\frac{\partial}{\partial t}(\rho\varepsilon) + \frac{\partial}{\partial x_i}(\rho\varepsilon u_i) = \frac{\partial}{\partial x_j}\left[\left(\mu + \frac{\mu_t}{\sigma_\varepsilon}\right)\frac{\partial \varepsilon}{\partial x_j}\right]$$

$$+C_{1\varepsilon}\frac{\varepsilon}{k}(G_k + C_{3\varepsilon}G_b) - C_{2\varepsilon}\rho\frac{\varepsilon^2}{k} + S_\varepsilon \tag{5}$$

G_k is the production of turbulent kinetic energy

$$G_k = -\rho\overline{u_i' u_j'}\frac{\partial u_j}{\partial x_i} \tag{6}$$

Effect of buoyancy

$$G_b = \beta g_i \frac{\mu_t}{\mathrm{Pr}_t}\frac{\partial T}{\partial x_i} \tag{7}$$

Where Pr_t is the turbulent Prandtl number for energy and g_i is the component of the gravitational vector in the i^{th} direction. For the standard and realizable - models, the default value of Pr_t is 0.85.

Y_M represents the expansion of the turbulent fluctuations. S and S_k are terms of sources.

$$Y_M = 2\rho\varepsilon M_t^2 \tag{8}$$

Turbulent viscosity is modeled as:

$$\mu_t = \rho C_\mu \frac{k^2}{\varepsilon} \tag{9}$$

$C_{\varepsilon 1}$, $C_{\varepsilon 2}$ and C_μ are constants that were determined experimentally and are given in table 1.
σ_ε and σ_k represents respectively the Prandtl number for turbulent kinetic energy and dissipation rate, these are also given in Table 1.

Table 1. Constant values of k –ε model

C_μ	$C_{\varepsilon 1}$	$C_{\varepsilon 2}$	σ_k	σ_ε
0.09	1.44	1.92	1	1.3

3.1.2 RNG k –ε Model

The RNG model, developed by the renormalization group (Yakhot & Smith) [19, 20] is an estimate in the calculation of the constant $C\varepsilon_1$, replaced in the equation of dissipation $C''_{\varepsilon 1}$. This expression adds a term function of strain rate η in the equation of dissipation, making it less diffusive.

$$\eta = \frac{k}{\varepsilon}\sqrt{\frac{p}{\eta_t}} \tag{10}$$

With

$$c''_{\varepsilon 1} = c_{\varepsilon 1} - \frac{\eta\left(1-\frac{\eta}{\eta_0}\right)}{1+\beta\eta^3} \tag{11}$$

The RNG model constants are given in Table2.

Table 2. Constant values of RNG k –ε model

C_μ	$C_{\varepsilon 1}$	$C_{\varepsilon 2}$	σ_ε	η_0	β
0.085	1.42	1.62	0.7179	4.38	0.015

The main difference between standard version and RNG k-ε is in the equation of the rate of turbulent dissipation of energy. In flows with high levels of constraint, the RNG model provides a low turbulent viscosity (that is to say a high dissipation rate ε and production of turbulence k low) than the standard model.
Although the RNG k-ε model was found to work better than the standard model for flows with large curvature of the streamlines, it has not yet been validated extensively by researchers opposed to the k-ε model. The standard version k - ε and RNG k-ε is valid for turbulent flows away from the walls.

3.1.3 Realizable k-epsilon model:

The realizable k-epsilon model is recently developed by Shih (1995); he uses another form of turbulent viscosity and dissipation equations [21, 22]:

$$\frac{\partial}{\partial t}(\rho k)+\frac{\partial}{\partial x_i}(\rho k u_i)=\frac{\partial}{\partial x_j}\left[\left(\mu+\frac{\mu_t}{\sigma_k}\right)\frac{\partial k}{\partial x_j}\right] + G_k + G_b - \rho\varepsilon - Y_M + S_K \tag{12}$$

$$\frac{\partial}{\partial t}(\rho\varepsilon)+\frac{\partial}{\partial x_i}(\rho\varepsilon u_i)=\frac{\partial}{\partial x_j}\left[\left(\mu+\frac{\mu_t}{\sigma_\varepsilon}\right)\frac{\partial \varepsilon}{\partial x_j}\right] + \rho C_1 S\varepsilon - \rho C_2\frac{\varepsilon^2}{k+\sqrt{\nu\varepsilon}} + C_{1\varepsilon}\frac{\varepsilon}{k}C_{3\varepsilon}G_b + S_\varepsilon \tag{13}$$

The turbulent viscosity is determined by the equation below, which is identical with the standard model, but in this model Cμ is variable.

$$\mu_t = \rho C_\mu \frac{k^2}{\varepsilon} \tag{14}$$

Where

$$C_\mu = \frac{1}{A_0 + A_s\frac{kU^*}{\varepsilon}} \tag{15}$$

$$U^* = \sqrt{S_{ij}S_{ij} + \widetilde{\Omega_{ij}}\widetilde{\Omega_{ij}}} \tag{16}$$

$$\widetilde{\Omega_{ij}} = \overline{\Omega_{ij}} - \varepsilon_{ijk}\omega_k - 2\varepsilon_{ijk}\omega_k \tag{17}$$

$\overline{\Omega_{ij}}$: The average rotation velocity

ω_k : Angular velocity

A_0=4.04 $\quad A_S = \sqrt{6}\cos\phi$

With:

$$\phi = \frac{1}{3}\cos^{-1}\left(\sqrt{6}\frac{S_{ij}S_{jk}S_{ki}}{\tilde{S}^3}\right) \tag{18}$$

$$\tilde{S} = \sqrt{S_{ij}S_{ij}} \tag{19}$$

$$S_{ij} = \frac{1}{2}\left(\frac{\partial u_j}{\partial x_i}+\frac{\partial u_i}{\partial x_j}\right) \tag{20}$$

The constants of this model are given in Table 3.

Table 3. Constant values of K-ε realizable model

$C_{\varepsilon 1}$	C_2	σ_k	σ_ε
1.44	1.9	0.7179	4.38

3.2 Calculation Domain: Boundary conditions

An Inlet boundary condition is used as flow is directed into the domain at location 'Inflow' shown in (Figure 2). Inlet velocity is taken as 0.26 m/s. Turbulence intensity I=u / U is 5% at inlet boundary condition in which, 'U' is the vector of velocity $U_{x,y}$ and 'u' being fluctuating velocity component in turbulent flow. At pressure outlets, the elevation of the water

must usually be known as part of the problem definition. The mechanism used to enforce this elevation is to set a pressure profile consistent with the known elevation. Top and bottom boundary are free slip condition. In this case, the velocity component parallel to wall has a finite value (which is computed), but the velocity normal to the wall, and wall shear stress, are both set to 0: $U_{N, Wall}=0$ and $\tau_w=0$. For 2-D both sides are taken as symmetry plane boundary condition which 'mirror' the flow on either side. The normal velocity component at the symmetry plane boundary and the scalar variable gradients normal to the boundary are set to zero.

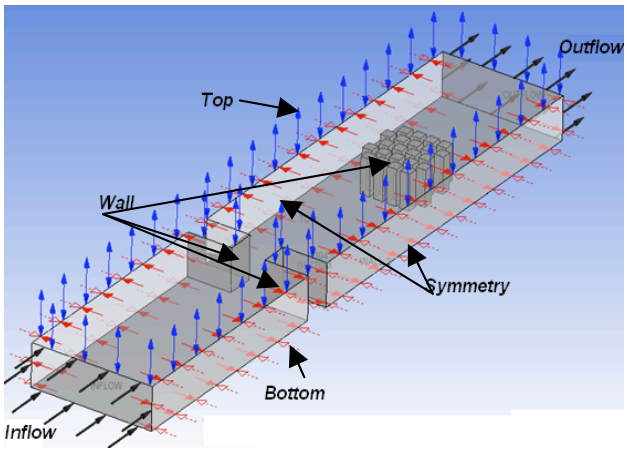

Fig. 2. Calculation domain showing 3D boundary conditions

3.3 Mesh Generation

To accurately predict the flow over the complex terrain, a great deal will depend on the good mesh generation, by keeping always in mind the importance of the memory and computing time. To capture the flow effects near the boundary wall of the ground, and to predict accurately the Water height, size and density of mesh are two parameters which have a major importance. According to the literature, three methods of mesh presented below (Figure 3 to 5), are among the recommended methods for calculating the fluid flow, each one has its advantages and disadvantages.

The first method consists to mesh the domain with unstructured tetrahedral mesh, using inflation option, from bottom to the estimated height of water (figure 3). Inflation refers to the generation of prism layers next to the wall to increase the resolution of gradients normal to the wall. This is accomplished with the boundary layer function in ANSYS-CFX mesh. In the second method, unstructured tetrahedral mesh has been exploited also, except near the boundary wall (obstacles walls, bottom) mesh refinement method has been employed instead of inflation method (Figure 4). In the third method, a structured hexahedral volume mesh in throughout domain is applied, fewer cells are needed for a hexahedral mesh, and the convergence is better (Figure 5).

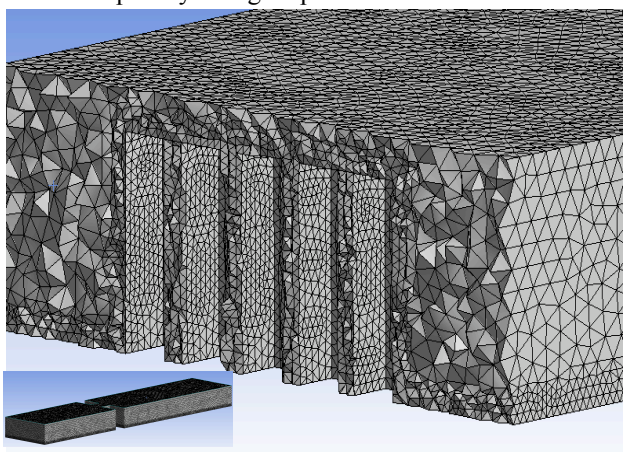

Fig. 3. Unstructured tetrahedral mesh with inflation

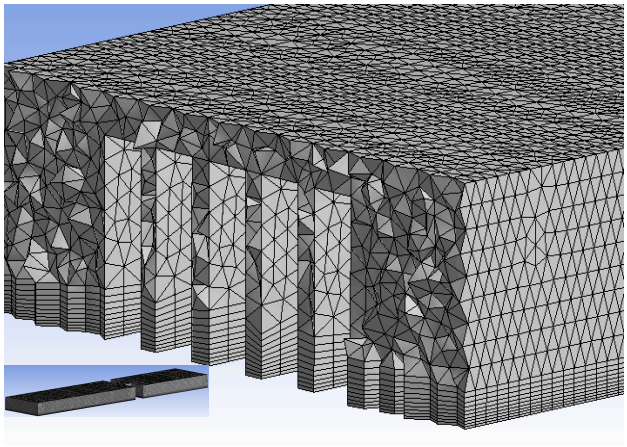

Fig. 4. Unstructured tetrahedral mesh with refinement

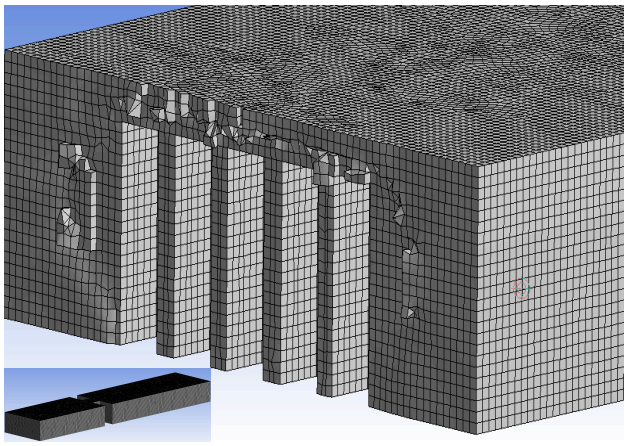

Fig. 5. Structured hexahedral mesh

In order to find the most suitable one of this study case, 9 simulation tests are performed as shown in the table 4.

Table 4. Plan of simulation

Types of mesh	Elements number	Turbulences model	Computing time(hour)
1	677653	k-epsilon	6.56
2	1388735	k-epsilon	9.1
3	655347	k-epsilon	7.45
1	677653	RNG K-epsilon	6.49
2	1388735	RNG K-epsilon	8.55
3	655347	RNG K-epsilon	7.45
1	677653	RSM	7.15
2	1388735	RSM	9.3
3	655347	RSM	7.22

With:

1: Unstructured tetrahedral mesh with inflation
2: Unstructured tetrahedral mesh with refinement
3: Structured hexahedral mesh

4 Results and discussion

4.1 Effect of mesh

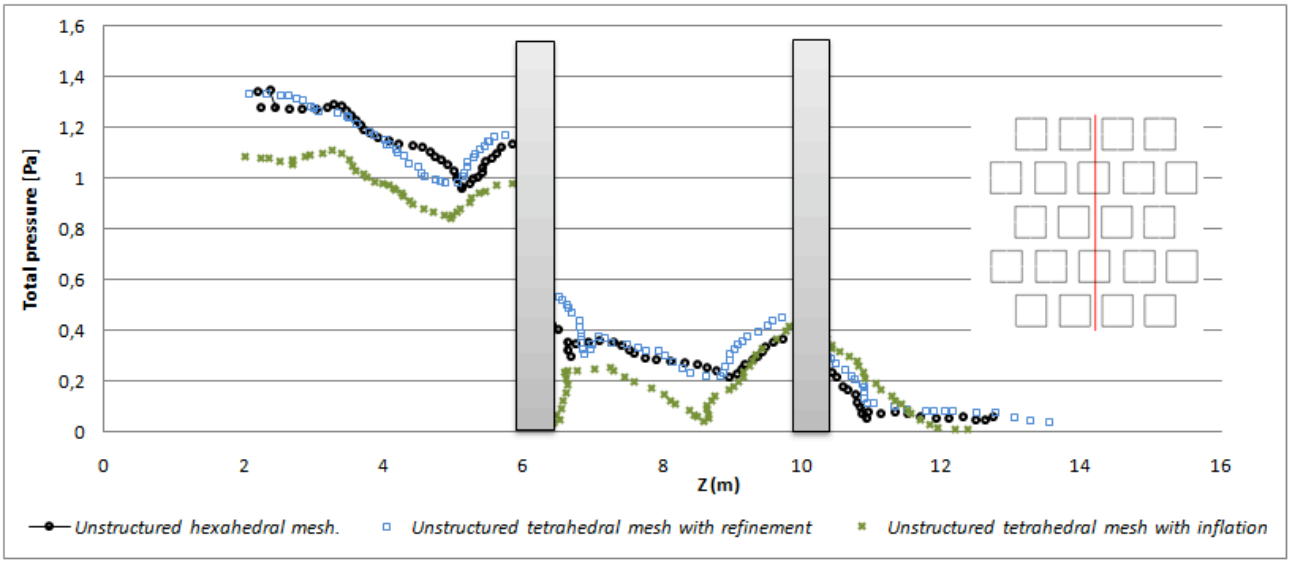

Fig. 6. Total pressure profiles according to type of mesh along Z axes.

A preliminary mesh convergence study is carried out in order to verify that the solution is meshing independent. Using the three meshing methods described above, it is found that for the same computing parameters and the same boundary conditions the results are deferent. The simulation is performed with the standard k-ε turbulence model for the three methods. Figure 6, shows the profiles of Total pressure along the Z axis. It is observed that the tetrahedral mesh with refinement and the hexahedral mesh methods give very similar profiles of pressure which differ numerically by less than 2%. The profile for the method of the tetrahedral volume mesh with inflation however, is clearly different, and numerically the results differ by up to 23%.

Figure 7 shows clearly the difference between the three results, depending on the meshing. Concerning the solutions (a, b), it is observed that pressure fields are so better between and around obstacles than in solution (c) , because of small size of elements mesh in this area.
It means that the tetrahedral mesh with refinement and the hexahedral mesh methods can provide more information about the behavior of the flow through the buildings network despite the complexity of the area. The maximum pressure values noticed in this area for different solutions (a, b, c) are: 420 Pa, 390 Pa, and 90 Pa respectively.

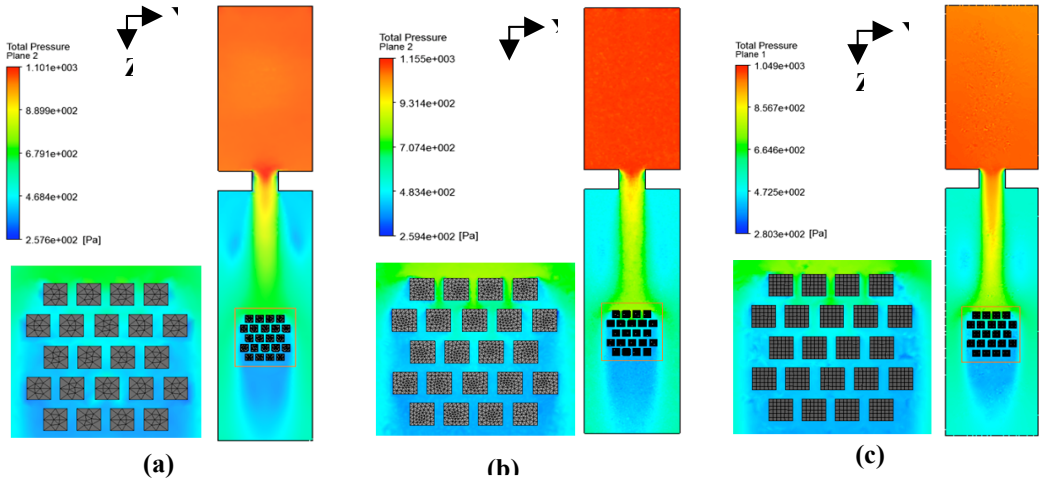

Fig. 7. Pressure field calculated for the three kinds of mesh in the ZX plan. (a)Unstructured tetrahedral volume mesh with inflation; (b) Unstructured tetrahedral volume mesh with refinement; (c) Structured hexahedral volume mesh

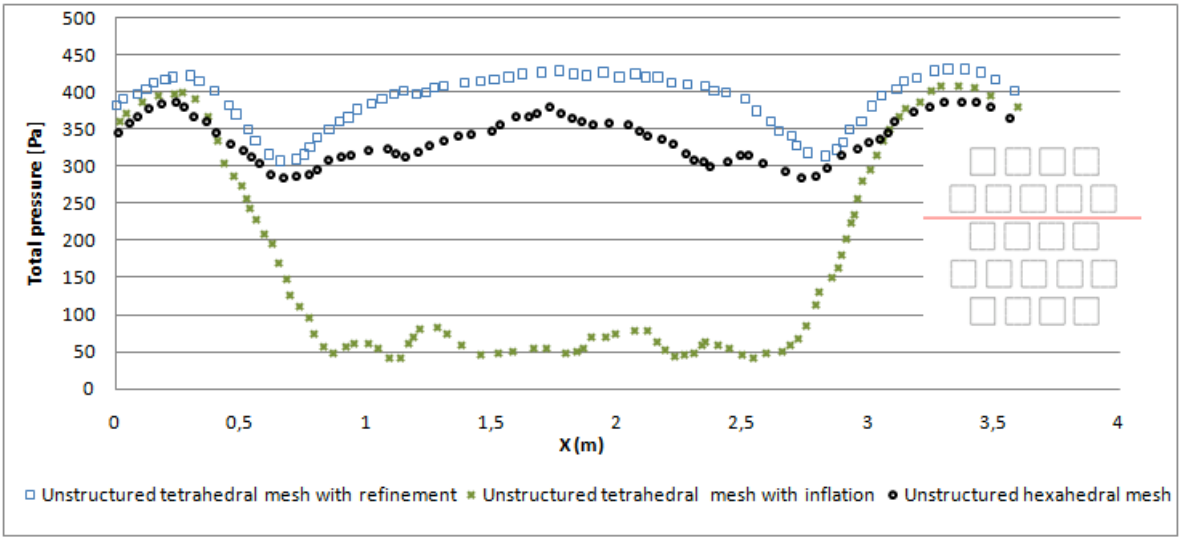

Fig. 8. Total pressure profiles according to type of mesh along X axes

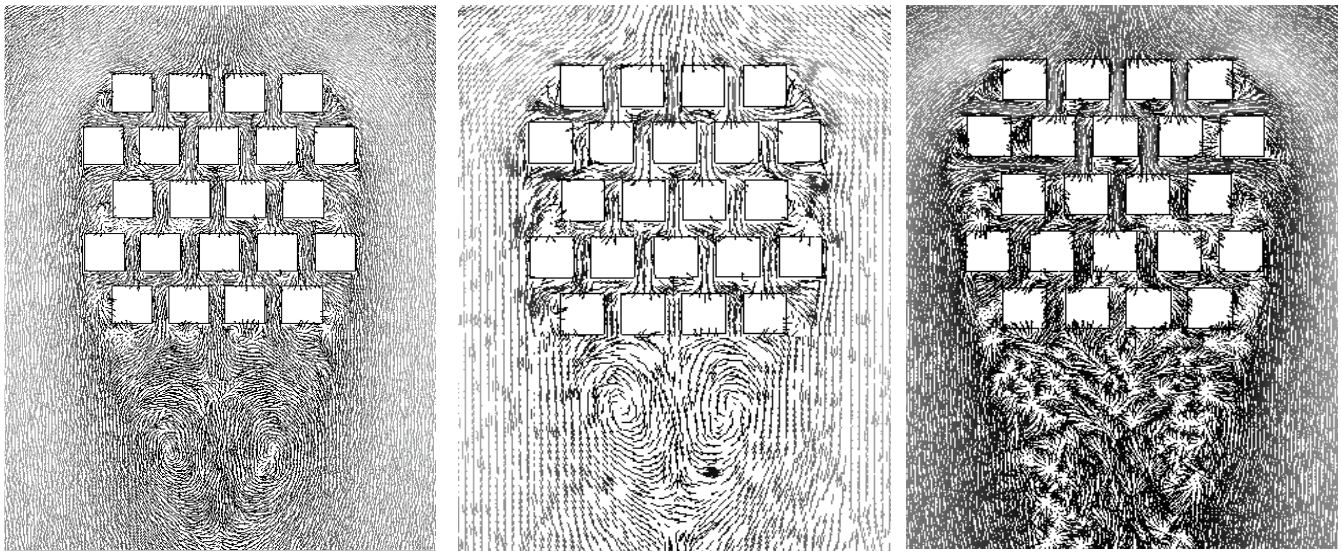

Fig. 9. Comparison between the velocity vectors simulated. (a) Standard k-ε; (b) RNG; (c) realizable k-ε

Figure 8 shows the profile of the total pressure along the X axis on the line just before the last group of buildings. It is remarked that the differences between the two simulations results for methods tetrahedral mesh with refinement and hexahedral mesh are minor. However, the hexahedral mesh method is employed for the simulation performed in this work is for reducing computational requirements.

4.2 Comparison of Turbulence Models

After the rapid opening of the gate, the strong dam-break wave reflects against the building, almost submerging it and the flow separates forming a series of shock waves crossing each other and creates a complicated flow structure, including several captured air pockets. Also, recirculation zones can be identified near the building.

4.2.1 Comparison of experimental and numerical velocity fields

The effect of the turbulence model was investigated using three isotropic models, the standard k-ε, Realizable k-ε and the RNG model. The experimental velocity vector plot using digital imaging technique [12] is compared with those of the three turbulence models in Figures 9.

In a general aspect, the two models RNG and standard k-ε, give flow patterns very alike (Figures 9 (a), (b)). They show almost similar field of vector velocity with the experimental one. This similitude is not observed with the realizable k-ε model, where it appears that the field of velocity vector behind the buildings is very disturbed and the velocity is close to zero.

Some small differences are noticed however between the two models; RNG and standard k-ε in the Distance of the onset of the vortex behind the group of buildings. Moreover the figure 10 shown the streamlines given by the three models, where there appears to be a slight deformation of the secondary circulation loop predicted by the RNG model behind the buildings , that is not observed with the standard k-ε model.

In the experiment performed, the Doppler velocimeter is placed in 9 points in the channel (Figure 11) and several measurements were made vertically. More the measuring point is near the urban area, the more the influence is strong and the differences between measure and simulation will be larger.

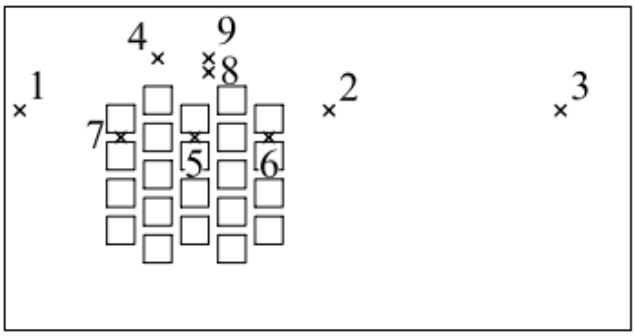

Fig.11. Positions of measurement points with Dopller velocimeter

Table 5 shows the measured and simulated values of the velocity vector in points 1, 2, 3, 4, 9 and 8 positioned in the channel as shown in Figure 11. At point 1, 4 and 9, the angle of the experimental velocity vector is almost constant and

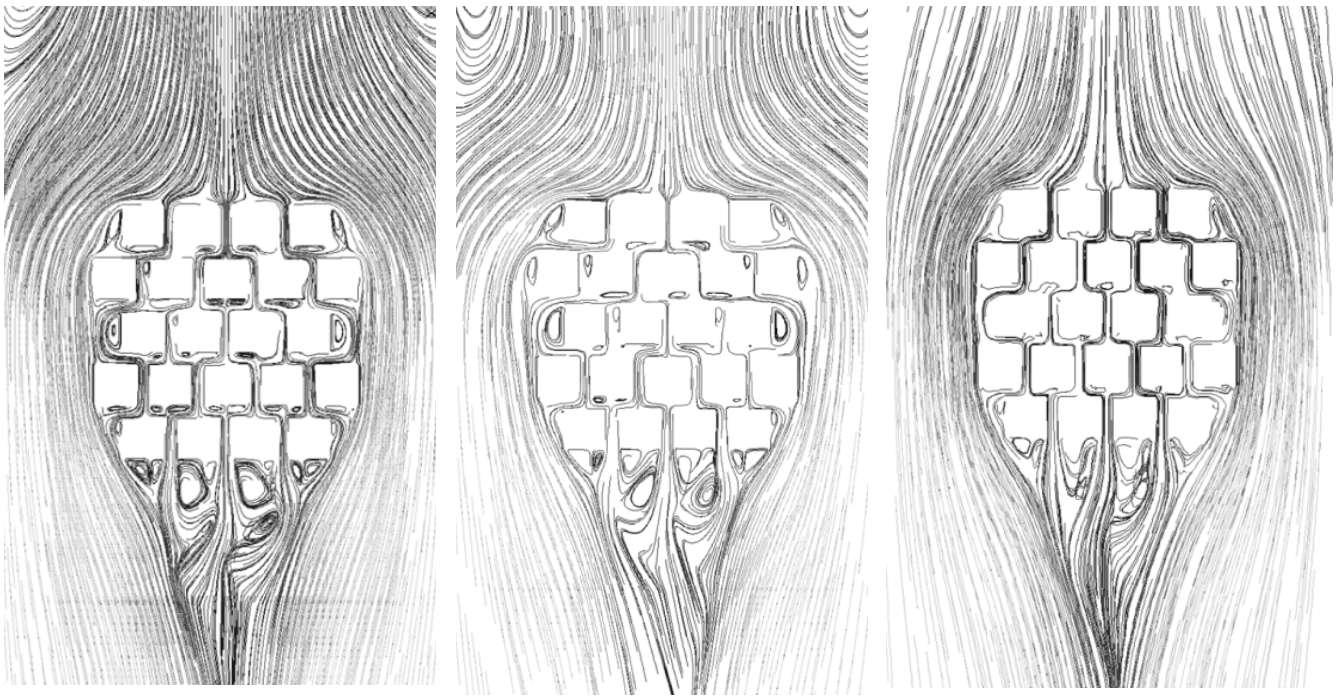

(a **(b)** **(c)**

Fig. 10. Streamlines with different simulated turbulence models. (a) Standard k-ε; (b) RNG; (c) realizable k-ε

very close to the angle of the velocity vector simulated with the all turbulences model. V_x and V_y velocity components simulated with realizable k-ε are slightly Higher than V_x experimental, while the V_x and V_y velocity components simulated with standard k-ε and RNG model are well estimated. The measuring point 2 is located in the recirculation zone located in the "wake" of the city. It is noticed that in Figure 10 (a) and (b) obtained by the RNG model and standard k-ε, two complete rotations of the velocity vector, whereas it is observed no complete rotation of the velocity vector simulated with the realizable k-ε model, but rather an oscillation generally between -90° and 90 °. The average of the V_x measured velocity component at point 2, is very close to zero (which is normal since the velocity vector is rotating), as the Vx simulated component.

The measuring point 3 is located 3m behind the urban area. Vy and Vx velocity components simulated are well estimated for every Turbulences model. The measuring point 8 is located on the same cross section as points 9, but it is a little closer to the urban area. The influence of the lateral recirculation (which occurs between the 2nd and 3rd row of buildings) is stronger. The values of the components of velocity simulated with standard k-ε and RNG turbulences model are very similar to the measured velocity vector. The Vx component simulated with realizable model is highly overestimated, while the Vy one is well estimated. The measuring points 5, 6 and 7 are located inside the urban area. With the simulation the flow enters the streets where are the three points, continuously at a velocity of 0.15 m / s, whereas from the experimental measurements of velocity components measured are almost nil. It can be explained by the fact that the width of the streets may be too low for the probe has a sufficient sample volume [12]. This shows that the simulated velocities with standard k-ε and RNG turbulences model are closer to the measured velocities (with some variation) than the realizable k-ε model.

4.2.2 Comparison of experimental and numerical profiles along the free surface

Table 5. The measured and simulated values of the velocity vector

Points	V_x and V_y Velocity	Experimental Values	Simulated values (standard k-ε)	Simulated values(RNG)	Simulated values (Realizable k-ε)
	v_x (m/s)	0,279	0,265	0,245	0,262
Point 1	v_y (m/s)	-0,086	-0,081	-0,072	-0,104
	v_x (m/s)	0,483	0,451	0,361	0,412
Point 4	v_y (m/s)	-0,074	-0,07	-0,066	-0,087
	v_x (m/s)	0,326	0,318	0,308	0,317
Point 9	v_y (m/s)	-0,005	-0,005	-0,004	-0,011
	v_x (m/s)	0,005	0,003	0,002	0,01
Point 2	v_y (m/s)	-0,037	-0,033	-0,020	-0,06
	v_x (m/s)	0,060	0,062	0,041	0,05
Point 3	v_y (m/s)	0,029	0,027	0,027	0,04
	v_x (m/s)	0,113	0,107	0,102	0,098
Point 8	v_y (m/s)	-0,013	-0,01	-0,012	-0,008

After the dam break, the water flows to the obstacles. Once it reaches this, a part of the wave is reflected and forms a negative bore travelling back in the upstream direction. The comparison between experimental and numerical results of the three turbulence models, in terms of free surface at different position along the longitudinal axis X is given in Figure 12.

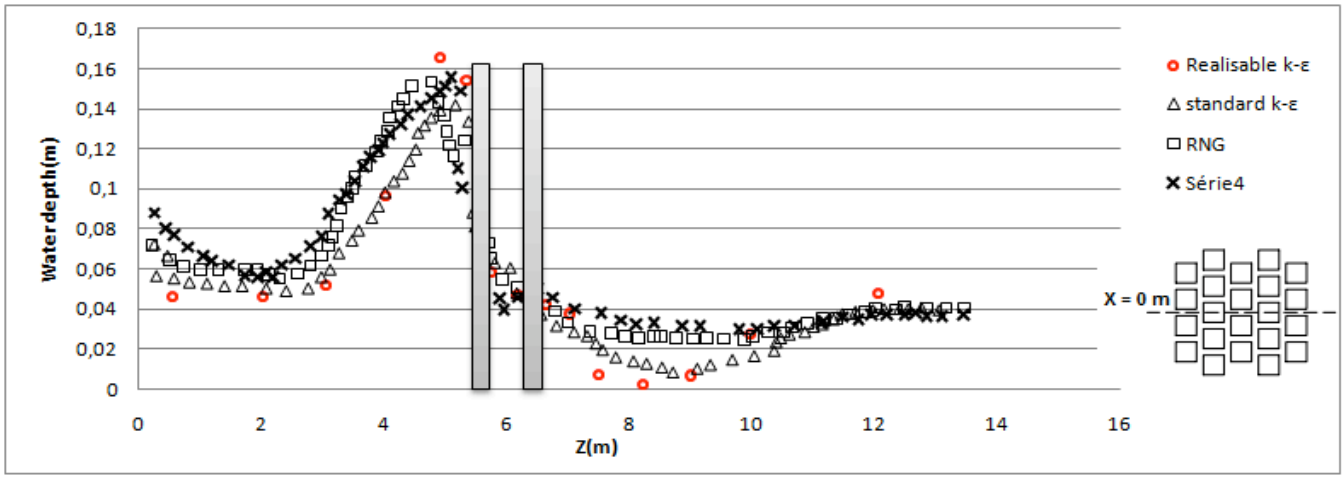

(a)

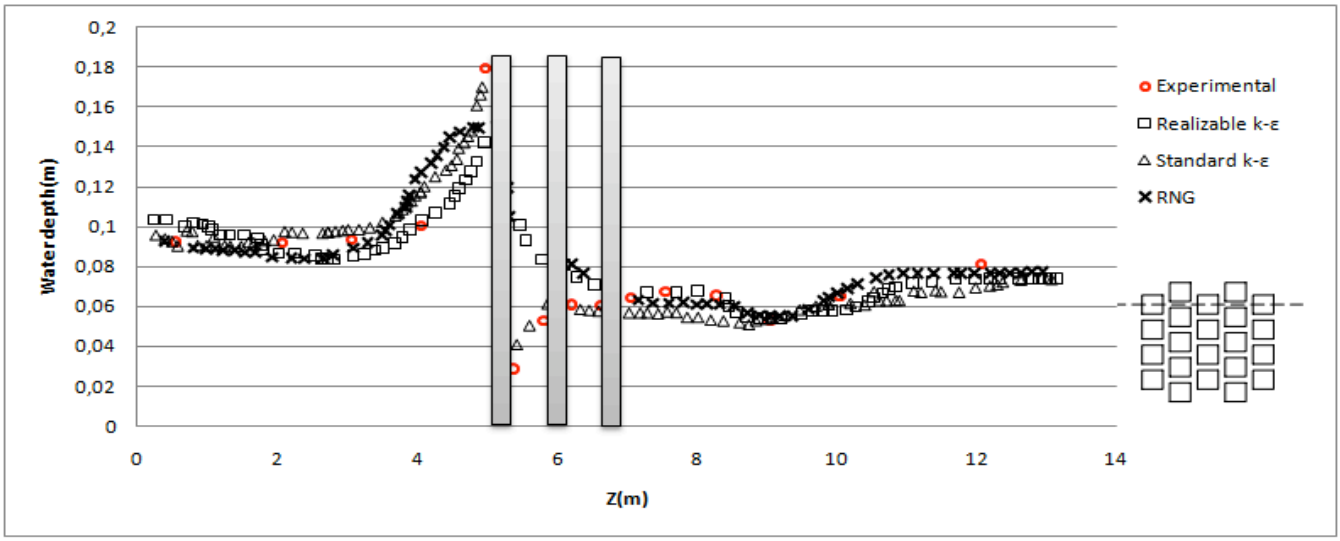

(b)

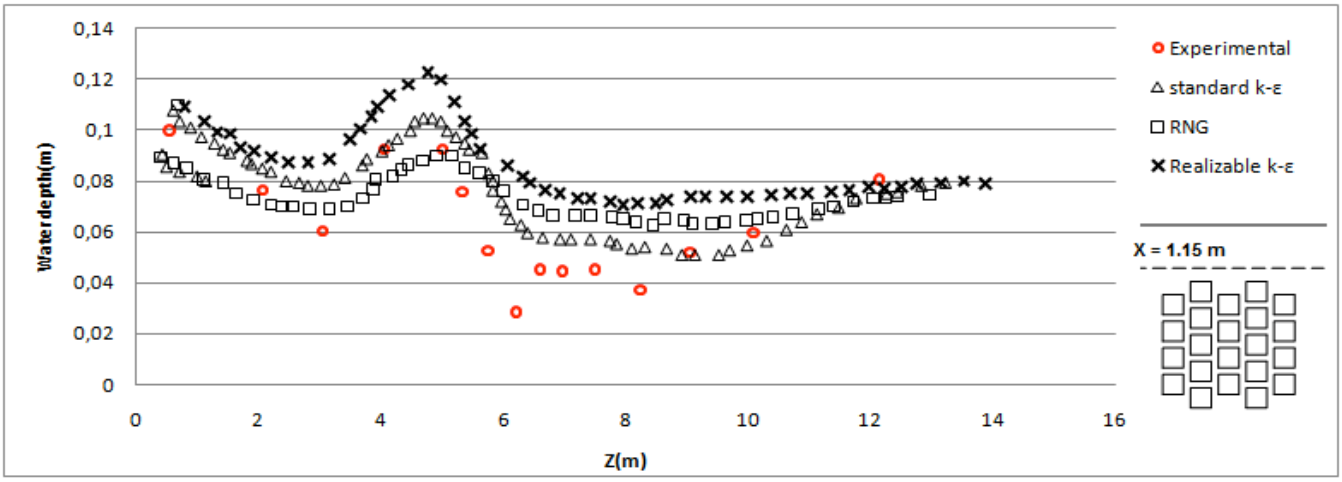

(c)

Fig. 12. Profiles along the free surface for the three turbulence models along the axis X. (a) For X = 0 m, (b) For X = 0.6m and (c) For X = 1.15m

The simulated free surface profiles are very close to that given by the measures experimental for any position of the X axis (Figure 13(a) X = 0m, 13(b)X = 0.6m, and13(c) X = 1.15m) but the standard k-ε seems to give the best profile. The free surface elevation upstream of the urban areas is well reproduced and it is less important along the axis z = 1.15 since it is located outside the urban area.

5 Conclusion

This study consist to show the influence of the different versions of K-epsilon turbulence model on the water flow behavior applied to three mesh types (hexahedral, tetrahedral with refinement and tetrahedral with inflation) predicted by Computational Fluid Dynamic (CFD) and validated through experiment. The summarizing pertinent results are:
Structured hexahedral mesh throughout the domain and k-epsilon model as a turbulence model can accurately represent the physical phenomena expected to occur in the real case of dam break such as turbulence zones near obstacles, and the free surface elevation upstream of the obstacle. The simulation results are in good agreement with the one obtained by experimental measure.
The set of results originating from these simulations shows that the dam break problem is characterized by three-dimensional aspects that have a great impact on water surface elevation and submersed wave travelling downstream.
The comparison between simulated and experimental results clearly shows that the three-dimensional model represents quite well the unsteady flow behavior.

References

1. J – M. Hervouet, R. Samie, B. Moreau. *Modelling urban areas in dam-break flood wave numerical simulations*. Proceedings of RESCDAM workshop. Seinäjoki, Finland: Finnish Environment Institute (2000).
2. Khan, R. Cadavid, S. S. Y. Wang. *Simulation of channel confluence and bifurcation using the CCHE2D model*. Water and Maritime Engineering. **142**, 97-102, (2000).
3. V. S. Neary, et F. Sotiropoulos. *Numerical investigation of laminar flows through 90-degree diversions of rectangular cross-section.* Computers and Fluids. **25**, 95-118, (1996).
4. L. S. Nania. PhD thesis: *Metodologia numérico-experimental para el analisis del riesgo asociado a la escorrentia pluvial en una redde calles*. Departamento de Ingéniera Hidraulica, Maritima y Ambiental Barcelona, Universitat politècnica de Catalunya (1999).
5. DHI Water and Environment, Reference Manual Mike Flood (2008). http://www.dhigroup.com, visited Marts 2008.
6. W. J. Sume. *Modelling of Bends and Hydraulic Structures in a Two-Dimensional Scheme*. Conference on Hydraulics in Civil Engineering, Hobart,. The Institution of Engineers, 28-30 (Australia, November 2001).
7. P. King, B.P. Donnel. Users Guide to RMA2 WES Version 4.5. US Army, Engineer research and Development Center. Waterways Experiment Station and Hydraulics Laboratory. USA (2006)
8. Deltares (2008), Reference Manual DELFT-FLS, http://www.wldelft.nl, visited Marts 2008.
9. S. Boonya-aroonnet, Č. Maksimović, D. Prodanović, S. Djordjević. *Urban pluvial flooding: development of GIS based pathway model for surface flooding and interface with surcharged sewer model,* Desbordes M. and B. Chocat (eds): Sustainable Techniques and Strategies in Urban Water Management. Proc. 6th Int. Conf. Novatech 2007, **1**, 481-488, France, (Lyon June 2007)
10. K. El Kadi Abderrezzak, A. Paquier and E. Mignot. *Modelling flash flood propagation in urban areas using a two-dimensional numerical model*, Natural Hazards, **50**, 433 - 460 (2009).
11. E. Mignot, A. Paquier and S. Haider, *Modeling floods in a dense urban area using 2D shallow water equations*, J. Hydrol., **327**(1-2), 186-199, (2006).
12. J. Lhomme, C. Bouvier, E.Mignot and A. Paquier. *One-dimensional GIS-based model compared to two-dimensional model in urban floods simulations*. Water Science and Technology, **54**(67), 83-91 (2006).
13. H. Capart, D. L. Young, Y. Zech. *Voronoï imaging methods for the measurement of granular flows*. Experiments in Fluids, **32**, 121-135, (2002).
14. D. B. Kothe, R. C. Mjolsness and M. D. Torrey. *RIPPLE: a computer program for incompressible flows with free surfaces*, Los Alamos National Laboratory, Report LA 12007 MS (1991).
15. P. Lin and P. L. -F. Liu. *Turbulence transport, vorticity dynamics, and solute mixing under plunging breaking waves in surfzone,* J. Geophys. Res., **103**, 15677-15694, (1998).
16. W. Rodi. *Turbulence Models and Their Application in Hydraulics*, International Association of Hydraulic Engineering (IAHR) Monograph, Delft, The Netherlands, (1980).
17. E. Launder and D. B. Spalding. *The numerical computation of turbulent flows*. Computer Methods in Applied Mechanics and Engineering. **3**, 269-289, (1974).
18. Y. Yang, M. Gu, S. Chen and X. Jin. *New inflow boundary conditions for modelling the neutral equilibrium atmospheric boundary layer in computational wind engineering*. Journal of Wind Engineering and Industrial Aerodynamics, **97**, 88-95 (2009).
19. V. Yakhot, S. A. Orszag. *Renormalization group analysis of turbulence*. Journal of Scientific Computing **1**, 3–51, (1986).
20. V. Yakhot, L. M. Smith, *The renormalization group, the ε-expansion and derivation of turbulence models*, J. Sci. Comput, **7**, 35-61, (1992).
21. T. –H. Shih, W. W. Liou, A. Shabbir and J. Zhu. A *New k-ε Eddy-Viscosity Model for High Reynolds Number Turbulent Flows - Model Development and Validation*, Computers & Fluids, **24**(3), 227-238 (1995).
22. C. Wilcox. Turbulence Modeling for CFD, 2nd Edition, DCW Industries, Inc (1988).